2012

PEGylated Silicon Nanowire Coated Silica Microparticles for Drug Delivery across Intestinal Epithelium

Vuk Uskoković
Chapman University, uskokovi@chapman.edu

Phin-Peng Lee
University of California - San Francisco

Laura Walsh
University of California - San Francisco

Kathleen Fischer
University of California - San Francisco

Tejal Dasai
University of California - San Francisco

Recommended Citation

Uskoković V, Lee P-P, Walsh L, Fischer K, Desai T. PEGylated silicon nanowire coated silica microparticles for drug delivery across intestinal epithelium. *Biomaterials*. 2012;33(5):1663-1672. doi:10.1016/j.biomaterials.2011.11.010.

PEGylated Silicon Nanowire Coated Silica Microparticles for Drug Delivery across Intestinal Epithelium

Published in final edited form as:
Biomaterials. 2012 February ; 33(5): 1663–1672. doi:10.1016/j.biomaterials.2011.11.010.

PEGylated Silicon Nanowire Coated Silica Microparticles for Drug Delivery across Intestinal Epithelium

Vuk Uskoković,
Therapeutic Micro and Nanotechnology Laboratory, Department of Bioengineering and Therapeutic Sciences, University of California, San Francisco, 1700 4th Street, San Francisco, CA 94158-2330, vuk.uskokovic@ucsf.edu

Phin-Peng Lee,
Therapeutic Micro and Nanotechnology Laboratory, Department of Bioengineering and Therapeutic Sciences, University of California, San Francisco, 1700 4th Street, San Francisco, CA 94158-2330, phinpeng@gmail.com

Laura Walsh,
Therapeutic Micro and Nanotechnology Laboratory, Department of Bioengineering and Therapeutic Sciences, University of California, San Francisco, 1700 4th Street, San Francisco, CA 94158-2330, laura.walsh@ucsf.edu

Kathleen Fischer, and
Therapeutic Micro and Nanotechnology Laboratory, Department of Bioengineering and Therapeutic Sciences, University of California, San Francisco, 1700 4th Street, San Francisco, CA 94158-2330, kayte.fischer@gmail.com

Tejal Desai
Therapeutic Micro and Nanotechnology Laboratory, Department of Bioengineering and Therapeutic Sciences, University of California, San Francisco, 1700 4th Street, San Francisco, CA 94158-2330, tejal.desai@ucsf.edu

Abstract

Composite particles made by growing nanoscopic silicon wires from the surface of monodispersed, microsized silica beads were tested in this study for their ability to affect the integrity and permeability of an epithelial cell layer. Polyethylene glycol (PEG) is known to sterically stabilize particles and prevent protein binding; as such, it is a routine way to impart *in vivo* longevity to drug carriers. The effect of the silica beads, both with and without silicon nanowires and PEG, on the disruption of the tight junctions in Caco-2 cells was evaluated by means of: (a) analysis of the localization of zonula occludens-1 (ZO-1), claudin-1 and f-actin; (b) measurements of trans-epithelial electrical resistance (TEER); (c) real-time quantitative RT-PCR analysis of the expression of *PKC*-α and *PKC-z*, which regulate the fluidity of cell membranes, and *RhoA* and *Rac1*, which are mainly involved in mechanotransduction processes; and (d) drug permeability experiments with fluorescein-sodium. The results have shown that Si-nanowire-coated silica microparticles added to Caco-2 cells in culture lead to alterations in tight junction permeability and the localization of ZO-1 and f-actin, as well as to decreased width of ZO-1 and claudin-1 at the tight junction and increased expression of *PKC* transcripts. Si-nanowire-coated

silica microparticles increased the permeability of Caco-2 cell monolayers to fluorescein-sodium in proportion to their amount. Effects indicative of loosening the Caco-2 cell monolayers and increasing their permeability were less pronounced for PEGylated particles, owing to their greater supposed inertness in comparison with the non-functionalized beads and nanowires. The analyzed Si-nanowire-coated silica microparticles have thus been shown to affect membrane barrier integrity in vitro, suggesting the possibility of using nanostructured microparticles to enhance drug permeability through the intestinal epithelium *in vivo*.

1. Introduction

Out of all routes for drug administration, oral remains the preferred one, and yet it suffers from many drawbacks, including the rapid clearing of the drug by the mucous layer and limited paracellular permeability through the epithelial lining of the gastrointestinal tract [1]. New devices are therefore actively being developed to overcome the low bioavailability of drugs administered orally [2–4]. Sufficient adhesion of these devices onto mucous surfaces is of great importance in achieving effective drug release over a prolonged period. Our previous work has shown that microsized silica beads coated with silicon nanowires present excellent candidates for adhesive drug delivery devices due to: (a) the facility of their loading with drug suspensions via the capillary effect; and (b) their ability to entwine with and sterically adhere to apical microvilli on the surface of epithelial cells [5–7].

In addition to improving the ability of drug delivery carriers to adhere to the apical side of the epithelium, it would be desirable to widen the intercellular junctions and enable more efficient paracellular transfer of the drug across the intestinal epithelial barrier. Tight junctions (TJs), the most apical intercellular structures in epithelial and endothelial cells, provide a crucial structural support to the epithelium, maintain the constitutive cells cohesive and polarized and are the rate-limiting factor for the kinetics of permeation of molecules across this layer [8]. The TJ, an essential pathway for the permeation of drugs across the epithelium of the gastrointestinal tract has the pore size of 1 – 3 nm, while the size of conventional water-soluble polymers or conglomerates of hydrophobic drug molecules ranges from few to several hundreds of nanometers [9]. Polymer-drug conjugates and molecular drugs *per se* whose size exceeds that of the pores of the TJ are therefore traditionally administered by intravenous means so as to avoid the need to cross the gastrointestinal epithelium. To develop drug delivery devices that can enhance oral bioavailability and increase the drug permeability of the TJ are major goals in pharmaceutical sciences.

In this work, we have tested silica beads, with and without silicon nanowires, in both their PEGylated and non-PEGylated forms, for their ability to affect the integrity and permeability of an *in vitro* model of the human intestinal epithelial layer in culture, which is a vital prerequisite for an effective transfer of the drug across the epithelium. Conjugation of drugs and drug delivery vehicles to polyethylene glycol (PEG) has been routinely used owing to the ability of conjugated PEG to: (a) sterically stabilize particles and prevent binding of plasma protein, thereby prolonging half-life in circulation and imparting *in vivo* longevity to the drug; (b) reduce immunogenicity; and (c) enhance permeability and retention effect [10]. PEG is also nontoxic, non-immunogenic, non-antigenic, highly soluble in water, FDA-approved, and has been shown to negligibly interfere with the drug release [11]. Caco-2, a human colon carcinoma cell line, was used in this work as an *in vitro* model for the intestinal epithelial barrier, the integrity of which was tested to the aforementioned drug delivery devices.

2. Methods

2.1. Silica beads (B) and silicon-nanowire-coated silica beads (NW)

NWs were provided by Nanosys, Inc., after being synthesized via a chemical vapor deposition of silicon ions onto silica beads sputtered with gold [12]. The beads were shown to be narrowly dispersed, having a diameter of 30 – 50 μm, while nanowires outgrown from the bead surface had the length of 5 – 10 μm and the diameter of circa 60 nm (See Supplementary Fig. 1).

2.2. PEGylated silica beads (B_{PEG}) and silicon-nanowire-coated silica beads (NW_{PEG})

The PEGylation protocol was adapted from Papra *et al* [13]. Hydroxylation of the particle surface was performed by keeping the particles at 80 °C for 5 min in a solution comprising 1.5 ml deionized (DI) H_2O, 0.3 ml NH_4OH and 0.3 ml H_2O_2. The particles were then cleaned at 80 °C for 5 min with a strong oxidizing solution containing 0.3 ml HCl and 0.3 ml H_2O_2 in 1.8 ml of DI H_2O. In-between these two steps, the particles were triply rinsed with water. After drying in ethanol, the particles were dispersed and aged for 3 h at room temperature in 2-[methoxy(polyethyleneoxy)propyl] methoxysilane (PEG silane, Mw = 460 – 590 g/mol, Gelest, Inc., Morrisville, PA). This was done by adding the particles into a plastic vial containing 3 ml toluene, 4.41 μl PEG silane and 2.4 μl HCl. After decanting the reactive solution, the particles were washed once in toluene, twice in ethanol and twice more in DI H_2O. A portion of the particles was then incubated in 20 μg/ml FITC-BSA for 2 h in dark to assess the surface coverage with PEG. A schematic presentation of the PEGylation process is given in Fig. 1.

2.3. Caco-2 Cell Culture

Caco-2 cell line, originally established in 1977 [14], has been a standard model system for assessing intestinal epithelial permeability [15] and has been previously proven as a useful model for the *in vitro* investigation of various drug delivery vehicles [16–18]. The human intestinal Caco-2 cells were obtained from American Tissue Culture Collection (ATCC, Rockville, MD) and cultured in Eagle's Minimum Essential Medium with Earle's Balanced Salt Solution, 1 mM sodium pyruvate, 20% fetal bovine serum (FBS), and 1% penicillin-streptomycin antibiotic solution. In all experiments, the cells were seeded in 24 well plates at a density of 7.5×10^4 cells/well on either collagen-coated glass cover slips (Fisherbrand®) or in the apical compartments of Transwells™. Every 7 days, the cells were detached from stock cultures by means of trypsin (0.25 wt%) digestion, washed, centrifuged (1000 rpm × 3 min), resuspended in 10 ml media and subcultured in 1:7 volume ratio. The cultures were regularly examined under an optical microscope to monitor their growth and possible contamination. Cell passages 3 – 24 were used for the hereby reported experiments.

2.4. Immunofluorescence for zonula occludens-1 (ZO-1), *claudin-1* and f-actin

Upon confluency, the Caco-2 cells were treated with 2 mg of particles in 500 μl of the cell culture media, and incubated for 2 – 6 h at 37 °C. The media with suspended particles were then removed and the cells were washed with phosphate buffer solution (PBS; pH 7.4) and fixed for either 15 min in 3.7 % paraformaldehyde (PFA) or 5 min in − 20 °C methanol. The cells were then washed three times with PBS, 5 min each, and then with the blocking solution (PBT = 1 % Bovine Serum Albumin (BSA), 0.1 % Triton X-100 in PBS) two times, 5 min each. The cells were then blocked and permeabilized in PBT for 1 h and then incubated with 200 μl/well primary antibody, 1:100 rabbit anti-ZO-1 (Zymed Lab) or 1:150 rabbit anti-claudin-1 (Abcam) in PBT overnight. After the overnight incubation, cells were washed with PBS 3 × 10 min and then incubated with 150 μl/well secondary antibody, 1:400 AlexaFluor 555 goat anti-rabbit (Invitrogen), phalloidin-tetramethylrhodamine (AlexaFluor

488, Invitrogen) and 4',6-diamidino-2-phenylindole dihydrochloride nuclear counterstain (DAPI, Invitrogen), all in PBT for one hour and then washed with PBS 3 × 5 min. The cover slips containing the fixed and stained cells were mounted onto glass slides using vectashield and imaged using a confocal laser scanning microscope – C1si (UCSF Nikon Imaging Center) at 10 – 100 × magnification. All the experiments were done in triplicates and the staining immunofluorescence pixel intensity was measured from four randomly selected images in each sample. Volume-rendered z-stack images (12 – 15 of them) spaced by 1 μm were collected at identical laser intensities and analyzed for the average pixel intensity using ImageJ and NIS Elements software. The thickness of claudin-1 conglomerates at the TJ was measured as half-width of peaks obtained by plotting the fluorescence intensity profiles across the cell boundary.

2.5. Real-time polymerase chain reaction (qPCR)

Confluent Caco-2 cells seeded in 24 well plates were treated with 2 mg of PEGylated particles (B_{PEG}, NW_{PEG}) and incubated for 2, 4 and 6 h. Cell lysis, reverse transcription (*Eppendorf*) and qPCR (*Applied Biosystems, StepONEPlus*) were performed using the Fast SYBR Green kit in accordance with the manufacturer's instructions. Each experiment was done in triplicates and each experimental replica was analyzed for mRNA expression in triplicates as well (n = 3 × 3). The expressions of four genes were analyzed: *GAPDH, PKC-α, PKC-z, RhoA,* and *Rac1*. The following primer pairs were used: *GAPDH* forward 5'-CTC TCT GCT CCT CCT GTT CG-3', reverse 5'-GCC CAA TAC GAC CAA ATC C-3'; *PKC-α* forward 5'-CAA GCA ATG CGT CAT CAA TGT-3', reverse 5'-TCC GCC CCC TCT TCT CA-3'; *PKC-z* forward 5'-CAC GCG TGA TTG ACC CTT TA-3', reverse 5'-CCC AGC CTG GCA TGC A-3'; *RhoA* forward 5'-CGG TCC TCC GTC GGT TCT-3', reverse 5'-ACG AAG GCG GGT AGC TGA A-3'; *Rac1* forward 5'-AGT GCT CGG CGC TCA CA-3', reverse 5'-CGG ATC GCT TCG TCA AAC A-3'. The real-time PCR results were analyzed using the ΔΔCt method [19] and all the data were normalized to *GAPDH* expression levels.

2.6. Trans-Epithelial Electrical Resistance (TEER) Measurements

Confluent Caco-2 cells seeded in high-density cell culture inserts with high pore density and 0.4 μm pore size (Falcon®) placed in 24 well plates were exposed apically to 2 mg of particles (B, NW, B_{PEG}, NW_{PEG}) in 500 μl of the cell culture media, and incubated for 24 h at 37 °C. Periodically, TEER values were read using an Epithelial Tissue Voltohmmeter (*EVOM, World Precision Instruments, Inc., Sarasota, FL*). The initial TEER was in the range of 500 – 700 Ωcm^2, which matched the earlier reported range of values for polarized monolayers of confluent Caco-2 cells as well as the typical values corresponding to the epithelial lining of the colon [20,21]. TEER values were measured before and during the 24 h treatment with the particles. The reported values present averages from four experimental replicas, each one of which was averaged from the results of 3 – 5 consecutive measurements. All the data points were normalized to the initial TEER for the given sample and compared with the control. Baseline measurements obtained by adding the same amount of particles to media in empty transwells showed the maximal increase in TEER of circa 25 Ohms for NW particles after 1 h, which was less than the typical change on the order of circa 100 Ohms observed for cell-seeded samples.

2.7. Fluorescein-sodium permeability across Caco-2 cell monolayers

Confluent Caco-2 cells seeded in high-density cell culture inserts with high pore density and 0.4 μm pore size (Falcon®) placed in 24 well plates were exposed apically to 4 mg of particles (NW, NW_{PEG}) in 500 μl of the phenol-free cell culture media containing 5 mg/ml of the model drug, fluorescein-sodium (Fluka). After 4 h of incubation at 37 °C, the basolateral compartments, initially containing pure PBS, were analyzed for their content of

the drug using a Packard Fluorocount™ fluorometer. The fluorescent model drug was detected with an excitation wavelength of 495 nm and an emission wavelength of 518 nm. All the experiments were done in quadruplicates and each experimental replica was analyzed for fluorescence in triplicates (n = 4 × 3). The initial TEER was in the range of 500 – 600 Ωcm^2 and its drop following the addition of the drug and the particles was assessed at different time points (0, 15 min, 30 min, 1 h, 2 h, 3 h, 4h). TEER was plotted as a function of time after normalization of values to the initial TEER for each given cell monolayer.

3. Results and discussion

Fluorescent optical micrographs of B and NW particles conjugated with FITC-BSA are shown in Fig. 2. PEGylated particles (B_{PEG}, NW_{PEG}) displayed markedly less fluorescence on their surface compared to the non-PEGylated ones (B, NW). The small amount of fluorescence from the PEGylated particles comes from the fact that PEGylation, even at Mw(PEG) as high as 6 kDa, does not completely shield the surface against protein adsorption [22].

The results of experiments designed to assess the effect of nanowire-coated silica beads on the permeability of a model drug compound, fluorescein-Na (376 Da), are shown in Fig. 3. A statistically significant increase in permeability of the drug with respect to the control was detected upon incubation of cell monolayers with both NW and NW_{PEG} (Fig. 3a), indicating that both of these types of particles are able to widen the TJ enough to promote increased permeation of a comparatively small molecule across the cell layer. The amount of the model drug that passed from the apical to the basolateral side of Caco-2 monolayers was, however, twice greater for NW than for NW_{PEG} (Fig. 3a), suggesting that PEGylation of the particles makes them more inert and less prone to alter the permeability of epithelial monolayer and promote greater flux of the drug across it. As can be seen from Fig. 3c, NW particles increase the drug permeability in direct proportion with the amount of NW added to the cell monolayers. As evident from Fig. 3b and Fig. 3d, the magnitude of decrease of TEER during incubation with the drug and the particles correlated with the permeability of the cell monolayers. The magnitude of increase in permeability (decrease in TEER), ranging at around 30–40 % difference with respect to the initial value for the drug alone, is comparable with the previous reports on the effect of drugs on TEER of Caco-2 cell layers [23,24]. After 4 h of incubation TEER values begin to stabilize and their partial recovery, to approximately 20 % of the initial value, is observed after 18 h (data not shown).

NW particles in combination with the drug thus induced a greater drop in TEER than NW_{PEG} particles coupled to the drug or the drug itself (Fig. 3b). Incubation with NW and NW_{PEG} particles *per se* also coincides with loosening of the cell monolayer indicated by a drop in TEER. The chemical nature of the coating of the particles, in this case PEG, can thus play an important role in determining the extent to which the particles can modulate paracellular permeability.

Following incubation with all of the four types of analyzed particles (B, NW, B_{PEG}, NW_{PEG}), cytoskeletal distribution of f-actin becomes altered as compared to control. As shown in Fig. 4, f-actin relocalizes to a certain extent to the vicinity of the cell membrane, as indicated by the transformation of its striated pattern that spans across multiple cells to a more cobblestone one. The transition from fibers traversing through the cytoplasm to their localization to the cell periphery is the possible consequence of the mechanochemical stress imposed by the particles onto the epithelial membrane [25]. Similar structural alterations of f-actin cytoskeleton, leading to its condensation in pericellular bands, have been previously observed under the effect of substances that disrupt the intestinal epithelial barrier [26]. In general, the cytoskeletal pattern of actin molecules in the perijunctional region of intestinal

epithelial cells tends to be either disrupted and modulated [27], or thickened and tightened [28] following incubation with particles or enteric biomolecules. As seen in Fig. 4, although filamentous actin is partially withdrawn to the cell periphery, no disruption in its cytoskeletal pattern is detected. Each cell is still surrounded by six other cells on average, as in agreement with the previous observations on the packing of confluent layers of Caco-2 cells [29]. This seems to indicate that while NW particles alter the TJ permeability, they do not disrupt the overall integrity of the monolayer.

Fig. 5 shows the typical cobblestone ZO-1 pattern following incubation with four types of particles (B, B_{PEG}, NW, NW_{PEG}) for 4 h. ZO-1 structure does not appear disrupted in comparison with the control for any of the particles. The average pixel intensity of ZO-1 fluorescence, however, is significantly increased for both types of PEGylated particles - B_{PEG} and NW_{PEG} (See Supplementary Fig. 2). Coinciding with the retraction of f-actin towards the cell membrane, the observed changes in the intensity of fluorescent ZO-1 following incubation with the NWs may be seen as indications of ongoing reorganization processes in the TJ region. This can be expected since actin microfilaments have insertion sites on junctional complexes and are engaged in interaction with the intercellular junctions [30]. Any disruption of the TJ, therefore, would result in a disruption of actin cytoskeletal network. ZO-1 has been, in fact, theorized to link the actin cytoskeleton to the TJ via an actin ZO-1 occludin complex [31]. Junctional and cytosolic proteins and actin microfilaments also interact with the C-terminal regions of the transmembrane proteins, contributing to the formation of the columnar epithelial sheet with regularly arranged nuclei and cell boundaries [32]. Specific drug treatments of epithelial cells have been shown previously to induce focal aggregation of TJ proteins which colocalize with disrupted actin at cell borders [33].

Comparison of the epithelium in contact with the four particles (B, B_{PEG}, NW, NW_{PEG}) with the untreated epithelium suggests no detectable damaging effects either to the TJ or to the epithelial integrity. Fig. 6a shows colocalization (yellow) of f-actin microfilaments stained in green and ZO-1 molecules immunostained in red. As shown in Fig. 6b, the TJ remains intact when in contact with a NW_{PEG} particle. No marked change in the density of the cell layer and the integrity of the cobblestone ZO-1 pattern was observed, suggesting no negative effects exerted on the cells by the given particles under the *in vitro* testing conditions applied herein. Moreover, ZO-1 localization does not appear to be disrupted when the amount of NW particles is increased from 10mg to 20mg (Fig. 6c–d).

The results of immunofluorescent staining of claudin-1 (Fig. 7), a member of the claudin family of transmembrane proteins (claudin-1 to -24), demonstrate effects on the intercellular pattern of claudin-1 molecules in confluent Caco-2 monolayers following a 4h incubation with the four types of analyzed particles (B, B_{PEG}, NW, NW_{PEG}). The non-PEGylated particles (B, NW; Fig. 7b,d) appear to have induced a decrease in the width of claudin-1 conglomerates that localize within the TJ zone (Figs. 7–8), which is suggestive of loosening of the TJ with respect to the control. In contrast, the same effect was absent when the cells were incubated with the PEGylated particles (B_{PEG}, NW_{PEG}; Fig. 7c,e). Unlike claudins-3 and -4 which undergo more striking smearing over the perpendicular projection on the epithelial cell monolayer following incubation with agents that alter paracellular permeability of Caco-2 cells [34], claudin-1 has been reported to change less in morphology, often exhibiting a similar drop in thickness at the TJ as observed hereby [35]. Over-expression of claudin-4 thus corresponds to increased permeability, while claudin-2 exhibits the opposite effect [36]; claudin-1, on the other hand, shows less drastic morphological changes upon altering the epithelial barrier. Different permeability enhancers were, for example, shown to induce narrower or more dispersed claudin-1 patterns in comparison with the control, depending on their chemical identity [37]. Still, decreased expression and down-

regulation of claudin-1 have been shown to correlate with increased permeability in Caco-2 cells [38,39], as in agreement with our findings. Conversely, an increased expression and smearing of claudin-1 molecules in the TJ zone often corresponds to decreased permeability [40,41] or recovery of the disrupted TJ following a particle treatment of Caco-2 cells.

The paracellular permeability is thought to be inversely proportional to the density of tight junctional strands [42–44]. A decreased density of claudin-1 molecules in the perijunctional domain following the treatment with the non-PEGylated particles could thus be indicative of higher paracellular permeability. In addition, each TJ strand can be treated as an individual resistor, while the overall TJ could be modeled as an additive series of electrical resistors. The increased amount of claudin-1 following incubation with the NW_{PEG} particles may thus be directly indicative of the comparatively higher electrical resistance measured using TEER (Fig. 3b). On the other hand, the lower width of claudin-1 conglomerates at the TJ observed after incubation with only non-PEGylated particles (B, NW) indicates their greater propensity to increase the paracellular permeability, as in agreement with the TEER results (Fig. 3b).

The real-time quantitative RT-PCR data in Fig. 9 show that already after 2 hours of incubation a significant up-regulation of both *PKC* genes has occurred in cells incubated with NW and NW_{PEG} (Fig. 9a–b). The overall up-regulation of *PKC* genes compared to both the control and cells treated with silica beads (B, B_{PEG}) was shown to be significantly more in cells treated with NW than in those incubated with NW_{PEG}. No statistically significant difference in the mRNA expression between B_{PEG}, NW_{PEG} and the control was detected for *RhoA* and *Rac1* at any of the time points (data not shown). Only when the amount of NW particles added to the cells was quadrupled, *Rac1* turns out to be up-regulated, along with *CDC42* (Fig. 9c). After 4 h of incubation, the expression of both *PKC*s in cells incubated with NW and NW_{PEG} becomes significantly higher compared to B_{PEG} and the control; no statistical difference ($p < 0.05$) was found between B_{PEG} and the control. At the same time, while the expression of *RhoA* and *Rac1* in cells incubated with NW_{PEG} is higher on average compared to B_{PEG} and the control, the higher expression levels were not statistically significant. Although *PKC* genes affect the TJ by controlling the contraction of apical acto-myosin filaments and coordinating the assembly of adherens junctions, respectively [45], *RhoA* and *Rac1* regulate many processes related to mechanotransduction, including cell migration processes [46]. Since no cell movement was detected and the integrity of the cell layer was preserved even at highest particle dosages (20 mg per well) and incubation times (24 h), little detectable change in expression of these genes was observed. *PKC* genes, on the other hand, express proteins involved in regulating epithelial permeability by maintaining the fluidity of the TJ [47]. Up-regulated expression of both *PKC*-α and *PKC-z* levels may thus correspond to the observed alteration of the ZO-1 intensity around the TJ, suggestive of increased paracellular permeability. In general, the more fluid the membrane, the greater the expression of *PKC*-α [48], a principle which is consistent with our findings. These results suggest that an altered expression of proteins involved in the assembly of the epithelial TJ is responsible for variations in its fluidity and permeability. Finally, *CDC42* is a GTPase that regulates f-actin polymerization and depolarization and its up-regulation corresponds to the earlier observed cytoskeletal reorganization following treatments with all types of particles (Fig. 4).

Based on the results presented here, we can only hypothesize about the reasons why PEGylated NW particles induce lesser loosening of the TJ in comparison with the non-PEGylated ones. To do so, the mechanochemical stress exerted by the particles could be divided to its mechanical and chemical elements. As for the former, it could be presumed that the soft polymeric “shield” of PEG lowers the direct mechanical effect of stiffer silicon nanowires and thus reduces their penetrative effect on the TJ. PEG coatings also appear to

affect the cell mechanotransduction pathways by avoiding recognition by surface integrins [49]. As far as the chemical perspective is concerned, the greater biochemical inertness of non-ionic PEG in comparison with the polar, wettable and more reactive oxidized and hydroxylated surface of Si nanowires and gold islands on their tips may explain the observed disparity. For example, microfluidic biosensing devices made of silicon can be coated with PEG so as to minimize the undesired adsorption of proteins onto the microchannel walls [50,51]. Owing to its protein-repellant nature, PEG resists binding of adjacent biomolecules [52], an effect which would presumably contribute to the entropic reduction and tightening of the TJ in contact with a PEGylated surface. The addition of a chemically inert, comparatively hydrophobic compound to an aqueous environment results in reduced entropy of the solvent, i.e., in a more rigid and ordered network of hydrogen bonds in the vicinity of the hydrophobic molecules [53]. By analogy, we could propose a similarly direct proportionality between the repulsive inertness of a compound and its effect on restricting the freedom of movement of the adjacent intercellular junctions, leading to their tightening. Previous studies have thus come to conclusion that alcoholic residues of H_2-antagonists, all of which "tighten" the TJ and reduce the epithelial permeability, had no effect on TEER in Caco-2 cells, whereas amine fragments caused an increase in TEER, suggestive of constricted intercellular spaces of these *in vitro* models of the intestinal mucous linings [54]. On the other hand, singular and associated $–OH^–$ and -O- groups on the surface of silicon in aqueous media could make the surface more prone to adherence of biomolecules, which leads to loosening of the TJ in contact with it. Surface charge effects are also known to be crucial in determining the cellular uptake of particles [55,56] and their disruptive or integrating effect on the TJ and the cytoskeleton [57]. The surface of cells and most biomolecules is negatively charged, favoring interaction with positively charged surfaces [58]. Our previous studies have shown that neutralization of positively charged surface of silicon nanowires following their conjugation with PEG reduces the adhesion of particles to Caco-2 cells [5]. A lesser surface charge of PEG in comparison with silicon and gold [59] may thus present yet another factor that contributes to its lesser reactivity with the perijunctional molecules and the smaller effect it has on loosening of the TJ.

4. Conclusion

In this study we evaluated the localization of f-actin filaments, zonula occludens-1 and claudin-1, indicative of the structure of the tight junction, in response to treatment with silicon-nanowire-coated silica particles, with and without PEG conjugation. These protein localization studies were carried out alongside the assessment of the effect of the given particles on the permeability of Caco-2 cell monolayers. The non-PEGylated particles were shown to loosen the tight junction in Caco-2 cells in culture to a greater extent than the PEGylated ones, as indicated by: (a) lower ZO-1 and claudin-1 intensities in the tight junction region; (b) lower width of ZO-1 and claudin-1 conglomerates at the tight junction; (c) more pronounced up-regulation of *PKC* transcripts; (d) greater drop in TEER values; (e) relocalization of f-actin cytoskeletally to the cell membrane and co-localizing with ZO-1; and (f) increased permeability of the Caco-2 cell monolayer to a model drug, fluorescein-sodium. The analyzed silicon-nanowire-coated silica microparticles were shown to not disrupt the overall membrane barrier integrity *in vitro*, but still allow for enhanced particle adhesion and drug permeability. The results of this study demonstrate that morphology on the nanoscale is an important consideration, in addition to chemistry, when it comes to design of advanced trans-epithelial drug delivery carriers.

Supplementary Material

Refer to Web version on PubMed Central for supplementary material.

Acknowledgments

Confocal microscopy data for this study were acquired at the Nikon Imaging Center at UCSF. This research was conducted with funding from the NIH Grant EB01166401. We thank Nanosys, Inc. for fabrication of the nanowire particles. The authors would like to acknowledge Kimberly Kam and Victoria M. Wu, both of UCSF, for useful discussions and help with the cell culture aspects of the study.

References

1. Morishita M, Peppas NA. Is the oral route possible for peptide and protein drug delivery? Drug Discov Today. 2006; 11:905–910. [PubMed: 16997140]
2. Tao SL, Desai TA. Gastrointestinal patch systems for oral drug delivery. Drug Discov Today. 2005; 10:909–915. [PubMed: 15993810]
3. Ahmed A, Bonner C, Desai TA. Bioadhesive microdevices with multiple reservoirs: a new platform for oral drug delivery. J Control Release. 2002; 81:291–306. [PubMed: 12044568]
4. Colombo P, Sonvico F, Colombo G, Bettini R. Novel platforms for oral drug delivery. Pharm Res. 2009; 26:601–611. [PubMed: 19132514]
5. Fischer KE, Nagaraj G, Daniels RH, Li E, Cowles VE, Miller JL, et al. Hierarchical nanoengineered surfaces for enhanced cytoadhesion and drug delivery. Biomaterials. 32:3499–3506. [PubMed: 21296409]
6. Fischer KE, Jayagopal A, Nagaraj G, Daniels R, Li E, Silvestrini M, et al. Nanoengineered surfaces enhance drug loading and adhesion. Nano Lett. 2011; 11:1076–1081. [PubMed: 21280638]
7. Fischer KE, Aleman BJ, Tao SL, Daniels RH, Li EM, Bunger MD, et al. Biomimetic nanowire coatings for next generation adhesive drug delivery systems. Nano Lett. 2009; 9:716–720. [PubMed: 19199759]
8. Schlegel N, Meir M, Heupel WM, Holthofer B, Leube RE, Waschke J. Desmoglein 2-mediated adhesion is required for intestinal epithelial barrier integrity. Am J Physiol- Gastr L. 2010; 298:G774, G783.
9. Kitchens K, Kolhatkar R, Swaan P, Eddington N, Ghandehari H. Transport of poly(amidoamine) dendrimers across Caco-2 cell monolayers: influence of size, charge and fluorescent labeling. Pharm Res. 2006; 23:2818–2826. [PubMed: 17094034]
10. Fishburn CS. The pharmacology of PEGylation: balancing PD with PK to generate novel therapeutics. J Pharm Sci. 2008; 97:4167–4183. [PubMed: 18200508]
11. Kouchakzadeh H, Shojaosadati SA, Maqhsoudi A, Farahani EV. Optimization of PEGylation conditions for BSA nanoparticles using response surface methodology. AAPS PharmSciTech. 2010; 11:1206–1211. [PubMed: 20680708]
12. Nanosys, Inc. Systems and methods for nanowire growth. US Patent. No. 20090124034. 2009.
13. Papra A, Gadegaard N, Larsen NB. Characterization of ultrathin poly(ethylene glycol) monolayers on silicon substrates. Langmuir. 2001; 17:1457–1460.
14. Fogh J, Fogh JM, Orfeo T. One hundred and twenty seven cultured human tumor cell lines producing tumors in nude mice. J Natl Cancer Inst. 1977; 59:221–226. [PubMed: 327080]
15. Hidalgo IJ, Raub TJ, Borchardt RT. Characterization of the human colon carcinoma cell line (Caco-2) as a model system for intestinal epithelial permeability. Gastroenterology. 1989; 96:736–749. [PubMed: 2914637]
16. Yu D, Marchiando AM, Weber CR, Raleigh DR, Wang Y, Shen L, et al. Mlck-dependent exchange and actin binding regiondependent anchoring of zo-1 regulate tight junction barrier function. PNAS. 2010; 107:8237–8241. [PubMed: 20404178]
17. Bimbo LM, Makila E, Laaksonen T, Lehto VP, Salonen J, Hirvonen J, et al. Drug permeation across intestinal epithelial cells using porous silicon nanoparticles. Biomaterials. 2011; 32:2625–2633. [PubMed: 21194747]
18. Neumeyer A, Bukowski M, Veith M, Lehr CM. Propidium iodide labeling of nanoparticles as a novel tool for the quantification of cellular binding and uptake. Nanomed-Nanotechnol. 2011; 7:410–419.

19. Pfaffl MW. A new mathematical model for relative quantification in real-time RT-PCR. Nucleic Acids Res. 2001; 29:e45. [PubMed: 11328886]
20. Artursson P, Karlsson J. Correlation between oral drug absorption in humans and apparent drug permeability coefficients in human intestinal epithelial (Caco-2) cells. Biochem Bioph Res Co. 1991; 175:880–885.
21. Yasumatsu H, Tanabe S. The casein peptide Asn-Pro-Trp-Asp-Gln enforces the intestinal tight junction partly by increasing occludin expression in Caco-2 cells. Brit J Nutr. 2010; 104:951–956. [PubMed: 20482929]
22. Xu H, Yan F, Monson EE, Kopelman R. Room-temperature preparation and characterization of poly(ethylene glycol)-coated silica nanoparticles for biomedical applications. J Biomed Mater Res A. 2003; 64:870–879. [PubMed: 12926040]
23. Alhamoruni A, Lee AC, Wright KL, Larvin M, O'Sullivan SE. Pharmacological effects of cannabinoids on the Caco-2 cell culture model of intestinal permeability. J Pharmacol Exp Ther. 2010; 335:92–102. [PubMed: 20592049]
24. Yeh TH, Hsu LW, Tseng MT, Lee PL, Sonjae K, Ho YC, Sung HW. Mechanism and consequence of chitosan-mediated reversible epithelial tight junction opening. Biomaterials. 2011; 32:6164–6173. [PubMed: 21641031]
25. Fu YY, Sibley E, Tang SC. Transient cytochalasin-d treatment induces apically administered Raav2 across tight junctions for transduction of enterocytes. J Gen Virol. 2008; 89:3004–3008. [PubMed: 19008386]
26. Xu LF, Xu C, Mao ZQ, Teng X, Ma L, Sun M. Disruption of the f-actin cytoskeleton and monolayer barrier integrity induced by PAF and the protective effect of ITF on intestinal epithelium. Arch Pharm Res. 2011; 34:245–251. [PubMed: 21380808]
27. Finamore A, Massimi M, Devirgiliis LC, Mengheri E. Zinc deficiency induces membrane barrier damage and increases neutrophil transmigration in Caco-2 cells. J Nutr. 2008; 138:1664–1670. [PubMed: 18716167]
28. Tahara K, Samura S, Tsuji K, Yamamoto H, Tsukada Y, Bando Y, et al. Oral nuclear factor-κb decoy oligonucleotides delivery system with chitosan modified poly(d.l-lactideco-glycolide) nanospheres for inflammatory bowel disease. Biomaterials. 2011; 32:870–878. [PubMed: 20934748]
29. Moyes SM, Morris JF, Carr KE. Macrophages increase microparticle uptake by enterocyte-like Caco-2 cell monolayers. J Anat. 2010; 217:740–754. [PubMed: 20880316]
30. Kojima T, Sawada N, Yamamoto M, Kokai Y, Mori M, Mochizuki M. Disruption of circumferential actin filament causes disappearance of occludin from the cell borders of rat hepatocytes in primary culture without distinct changes of tight junction strands. Cell Struct Funct. 1999; 24:11–17. [PubMed: 10355874]
31. Fanning AS, Jameson BJ, Jesaitis LA, Anderson JM. The tight junction protein zo-1 establishes a link between the transmembrane protein occludin and the actin cytoskeleton. J Biol Chem. 1998; 273:29745–29753. [PubMed: 9792688]
32. Takehara M, Nishimura T, Mima S, Hoshino T, Mizushima T. Effect of claudin expression on paracellular permeability, migration and invasion of colonic cancer cells. Biol Pharm Bull. 2009; 32:825–831. [PubMed: 19420749]
33. Wittchen ES, Haskins J, Stevenson BR. Protein interactions at the tight junction. Actin has multiple binding partners, and zo-1 forms independent complexes with zo-2 and zo-3. J Biol Chem. 1999; 274:35179–35185. [PubMed: 10575001]
34. Sander GR, Cummins AG, Powell BC. Rapid disruption of intestinal barrier function by gliadin involves altered expression of apical junctional proteins. FEBS Letters. 2005; 579:4851–4855. [PubMed: 16099460]
35. Dickman KG, Hempson J, Anderson J, Lippe S, Zhao L, Burafoff R, et al. Rotavirus alters paracellular permeability and energy metabolism in Caco-2 cells. Gastrointest Liver Physiol. 2000; 279:G757–G766.
36. Takehara M, Nishimura T, Mima S, Hoshino T, Mizushima T. Effect of claudin expression on paracellular permeability, migration and invasion of colonic cancer cells. Biol Pharm Bull. 2009; 32:825–831. [PubMed: 19420749]

37. Suzuki T, Hara H. Difructose anhydride III and sodium caprate activate paracellular transport via different intracellular events in Caco-2 cells. Life Sci. 2006; 79:401–410. [PubMed: 16566947]
38. Langlois MJ, Bergeron S, Bernatchez G, Boudreau F, Saucier C, Perreault N, et al. The PTEN phosphatase controls intestinal epithelial cell polarity and barrier function: role in colorectal cancer progression. PLoS One. 2010; 5:e15742. [PubMed: 21203412]
39. Murphy EF, Jewell C, Hooiveld GJ, Muller M, Cashman KD. Conjugated linoleic acid enhances transepithelial calcium transport in human intestinal-like Caco-2 cells: an insight into molecular changes. Prostog Leukotr Ess. 2006; 74:295–301.
40. Suzuki T, Hara H. Quercetin enhances intestinal barrier function through the assembly of zonula occludens-2, occludin, and claudin-1 and the expression of claudin-4 in Caco-2 cells. J Nutr. 2009; 139:965–974. [PubMed: 19297429]
41. McGilligan VE, Wallace JM, Heavey PM, Ridley DL, Rowland IR. The effect of nicotine in vitro on the integrity of tight junctions in Caco-2 cell monolayers. Food Chem Toxicol. 2007; 45:1593–1598. [PubMed: 17399881]
42. Claude P. Morphological factors influencing transepithelial permeability: a model for the resistance of the zonula occludens. J Membrane Biol. 1978; 39:219–232. [PubMed: 641977]
43. Marcial MA, Carlson SL, Madara JL. Partitioning of paracellular conductance along the ileal crypt-villus axis: a hypothesis based on structural analysis with detailed consideration of tight junction-structure function relationships. J Membrane Biol. 1987; 80:59–70. [PubMed: 6481793]
44. Shen L, Weber CR, Raleigh DR, Yu D, Turner JR. Tight junction pore and leak pathways: a dynamic duo. Annu Rev Physiol. 2011; 73:283–309. [PubMed: 20936941]
45. Popoff MR, Geny B. Multifaceted role of Rho, Rac, Cdc42 and Ras in intercellular junctions, lessons from toxins. Biochim Biophys Acta. 2009; 1788:797–812. [PubMed: 19366594]
46. Miqeotte I, Grego-Bessa J, Anderson KV. Rac1 mediates morphogenetic responses to intercellular signals in the gastrulating mouse embryo. Development. 2011; 138:3011–3020. [PubMed: 21693517]
47. Fasano A. Regulation of intercellular tight junctions by zonula occludens toxin and its eukaryotic analogue zonulin. Ann NY Acad Sci. 2000; 915:214–222. [PubMed: 11193578]
48. Mashukova A, Wald FA, Salas PJ. Tumor necrosis factor alpha and inflammation disrupt the polarity complex in intestinal epithelial cells by a posttranslational mechanism. Mol Cell Biol. 2011; 31:756–765. [PubMed: 21135124]
49. Slater JH, Frey W. Nanopatterning of fibronectin and the influence of integrin clustering on endothelial cell spreading and proliferation. J Biomed Mater Res Part A. 2008; 87:176–195.
50. Sharma S, Desai TA. Nanostructured antifouling poly(ethylene glycol) films for silicon-based microsystems. J Nanosci Nanotechno. 2005; 5:235–243.
51. Popat KC, Desai TA. Poly(ethylene glycol) interfaces: an approach for enhanced performance of microfluidic systems. Biosens Bioelectron. 2004; 19:1037–1044. [PubMed: 15018959]
52. Gonzalez AL, Gobin AS, West JL, McIntire LV, Smith CW. Integrin interactions with immobilized peptides in polyethylene glycol diacrylate hydrogels. Tissue Eng. 2004; 10:1775–1786. [PubMed: 15684686]
53. Tinoco, I.; Sauer, K., Jr; Wang, KC. Physical chemistry: principles and applications in biological sciences. Third Edition. Englewood Cliffs, NJ: Prentice Hall; 1995.
54. Gan LSL, Yanni S, Thakker DR. Modulation of the tight junctions of the Caco-2 cell monolayers by h_2-antagonists. Pharm Res. 1998; 15:53–57. [PubMed: 9487546]
55. Hu C, Peng Q, Chen F, Zhong Z, Zhou R. Low molecular weight polyethylenimine conjugated gold nanoparticles as efficient gene vectors. Bioconjugate Chem. 2010; 21:836–843.
56. Cerebrian V, Martin-Saavedra F, Yague C, Arruebo M, Santamaria J, Vilaboa N. Size-dependent transfection efficiency of pei-coated gold nanoparticles. Acta Biomater. 2011; 7:3645–3655. [PubMed: 21704738]
57. Sha X, Yan G, Wu Y, Li J, Fang X. Effect of self-microemulsifying drug delivery systems containing labrasol on tight junctions in Caco-2 cells. Eur J Pharm Sci. 2005; 24:477–486. [PubMed: 15784337]

58. Uskoković V, Uskoković DP. Nanosized hydroxyapatite and other calcium phosphates: chemistry of formation and application as drug and gene delivery agents. J Biomed Mater Res B. 2011; 96B: 152–191.

59. Essa S, Rabanel JM, Hildgen P. Characterization of rhodamine loaded PEG-g-PLA nanoparticles (NPs): effect of poly(ethylene glycol) grafting density. Int J Pharm. 2011; 411:178–187. [PubMed: 21458551]

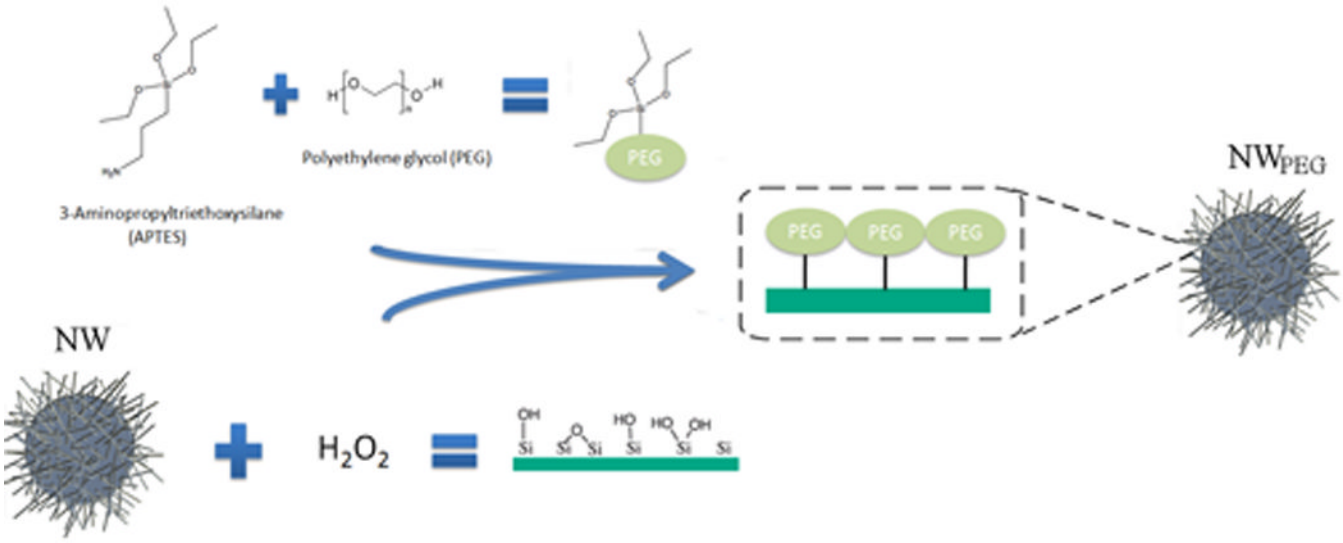

Fig. 1.
Schematic depiction of the process of PEGylation of NW particles.

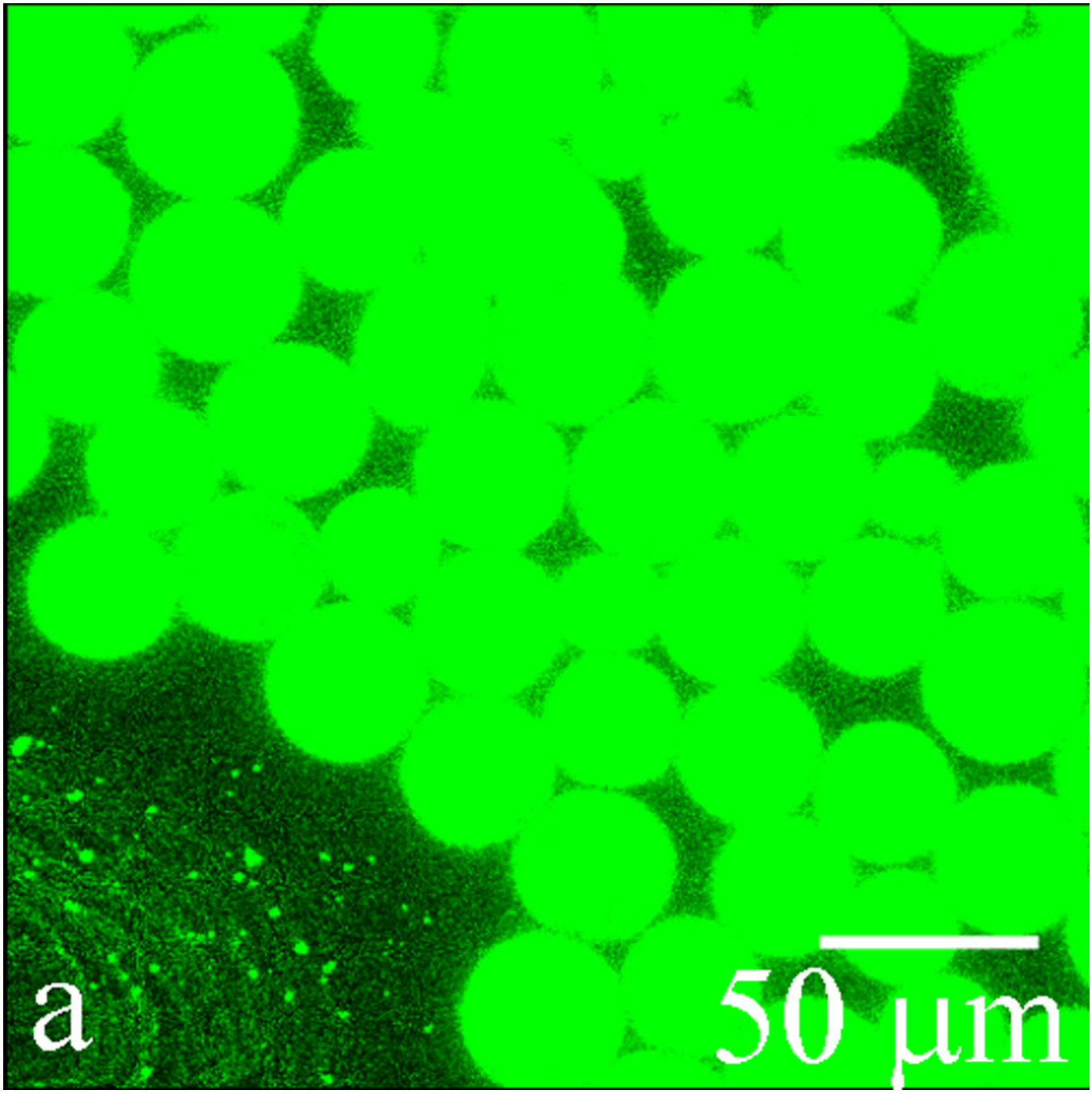

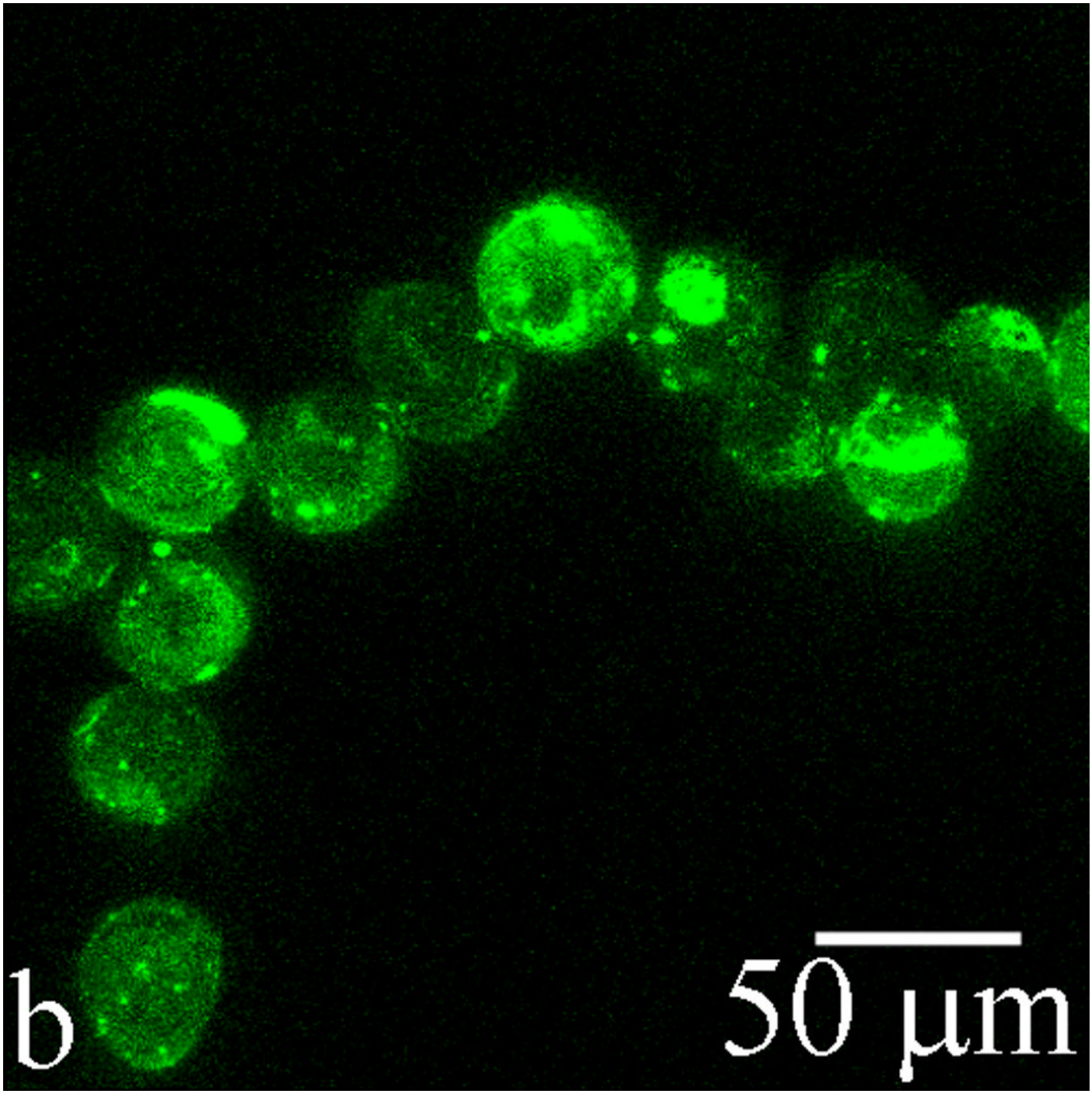

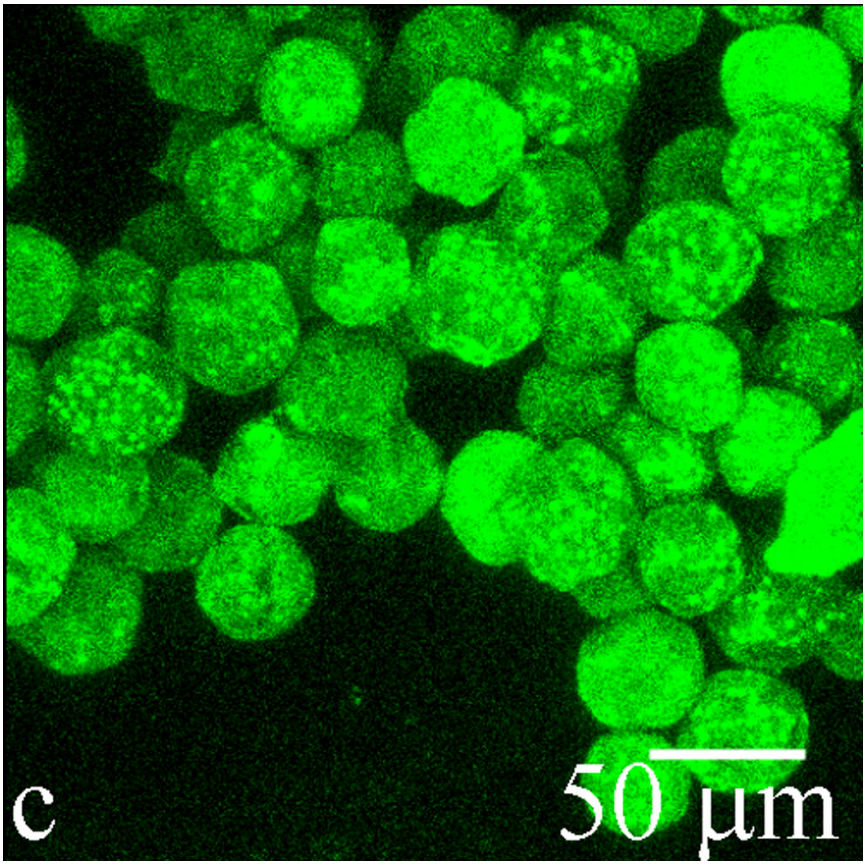

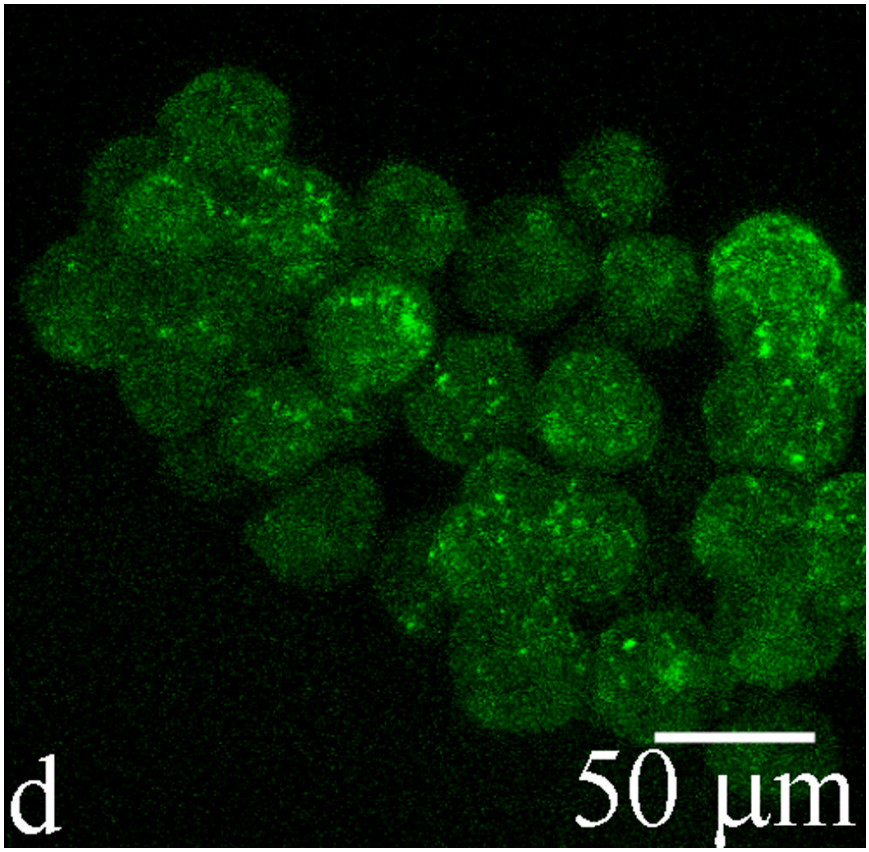

Fig. 2.
Confocal optical micrographs of B (a), B_{PEG} (b), NW (c), and NW_{PEG} (d) conjugated with FITC-BSA.

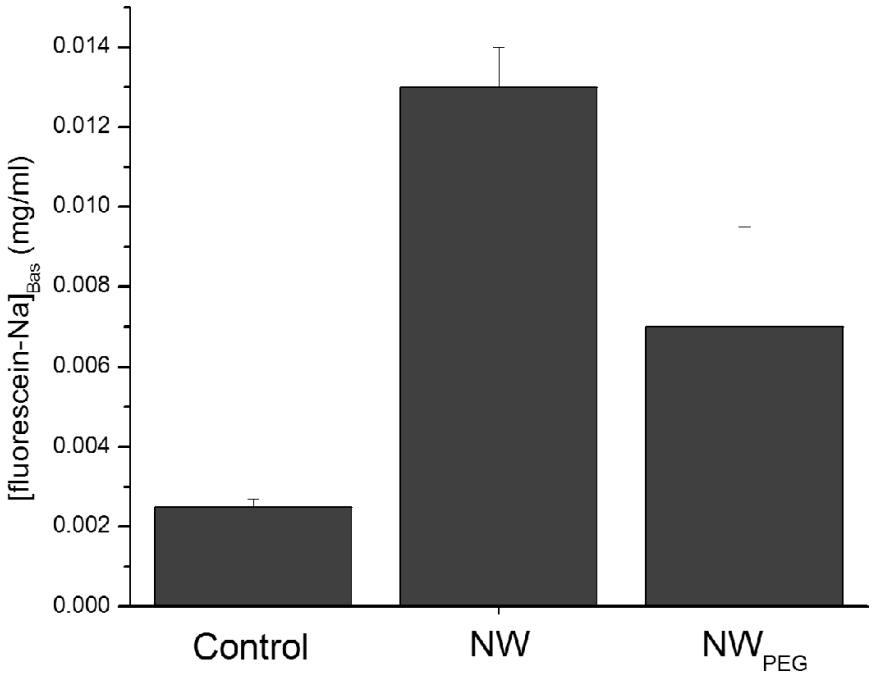

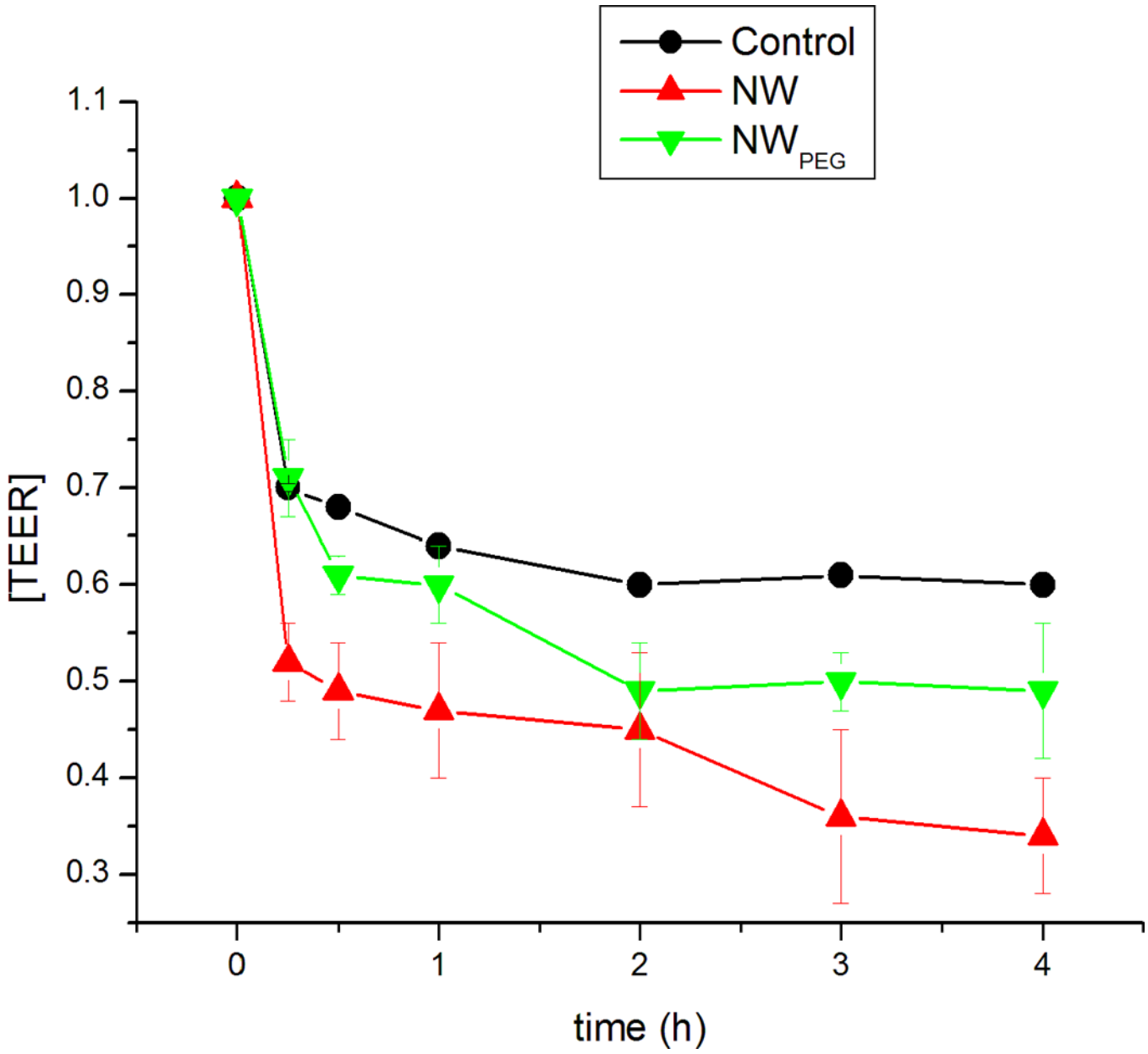

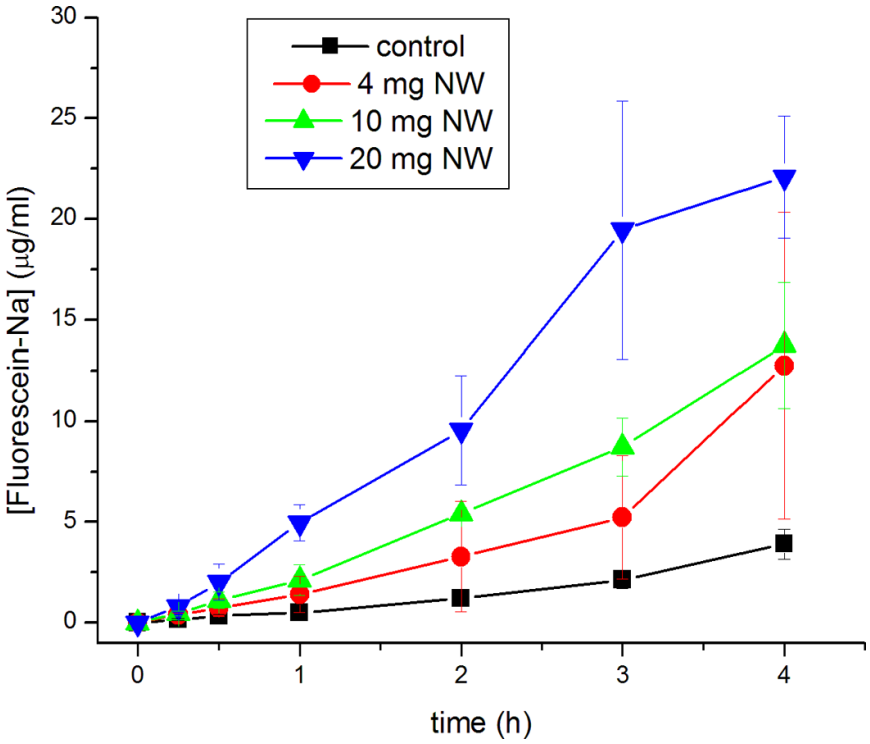

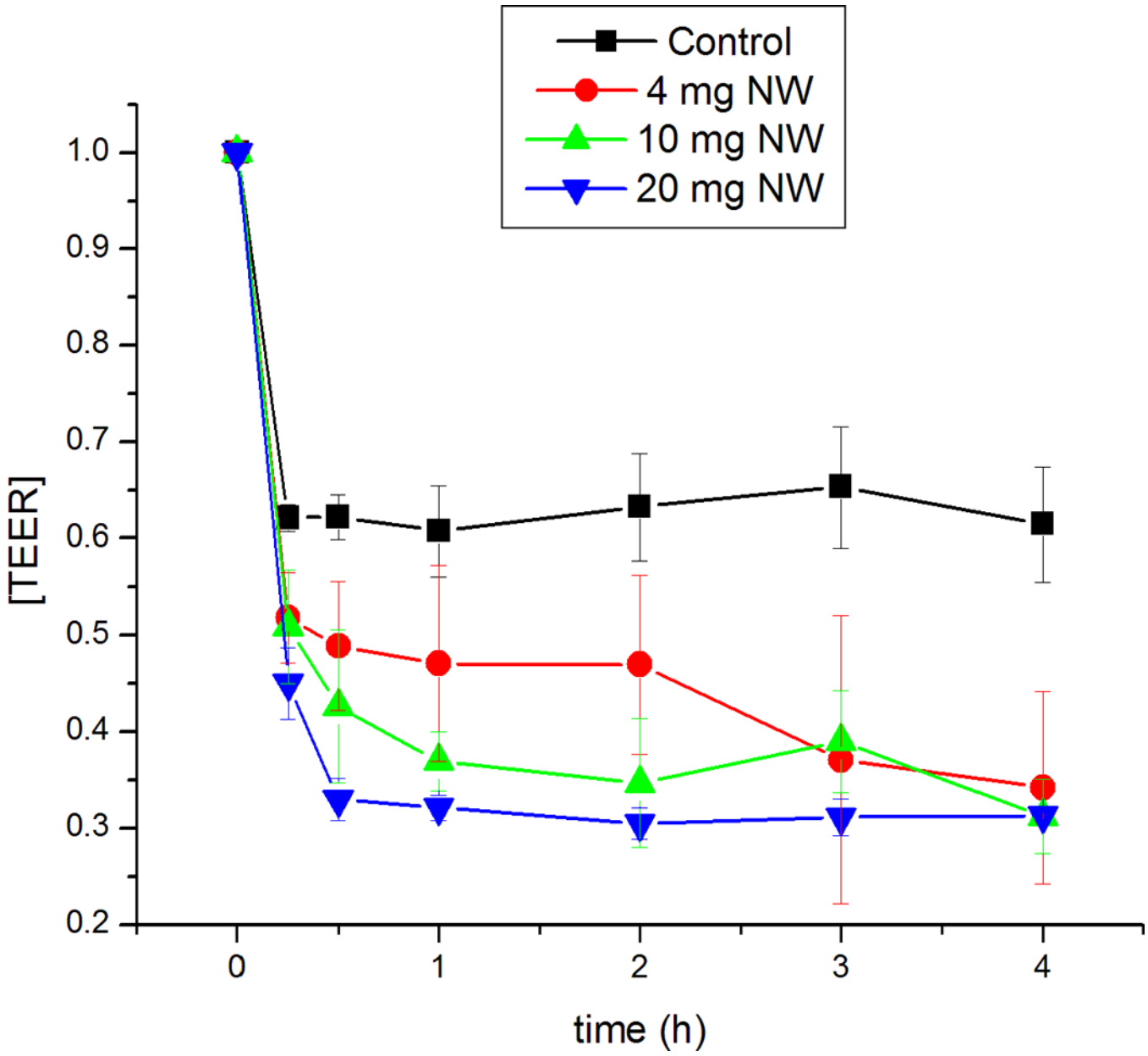

Fig. 3.

(a) Basolateral concentration of fluorescein-Na after 4 h of incubation time in the presence of NW and NW_{PEG}; (b) Normalized TEER of confluent Caco-2 cell monolayers as a function of the time of incubation with different types of particles (NW, NW_{PEG}) and fluorescein-Na in comparison with the control; (c) Basolateral concentration of fluorescein-Na during the first 4 h of incubation time in the presence of different amounts of NW per well; (d) Normalized TEER of confluent Caco-2 cell monolayers as a function of the time of incubation with different amounts of NW particles and fluorescein-Na in comparison with the control (two-way ANOVA test with replications indicated statistically significant ($p < 0.01$) difference between the following curves: control vs. 10mg; control vs. 20mg; 4mg vs. 10mg; 4mg vs. 20mg; 10mg vs. 20mg). Data are shown as means with error bars representing standard deviation.

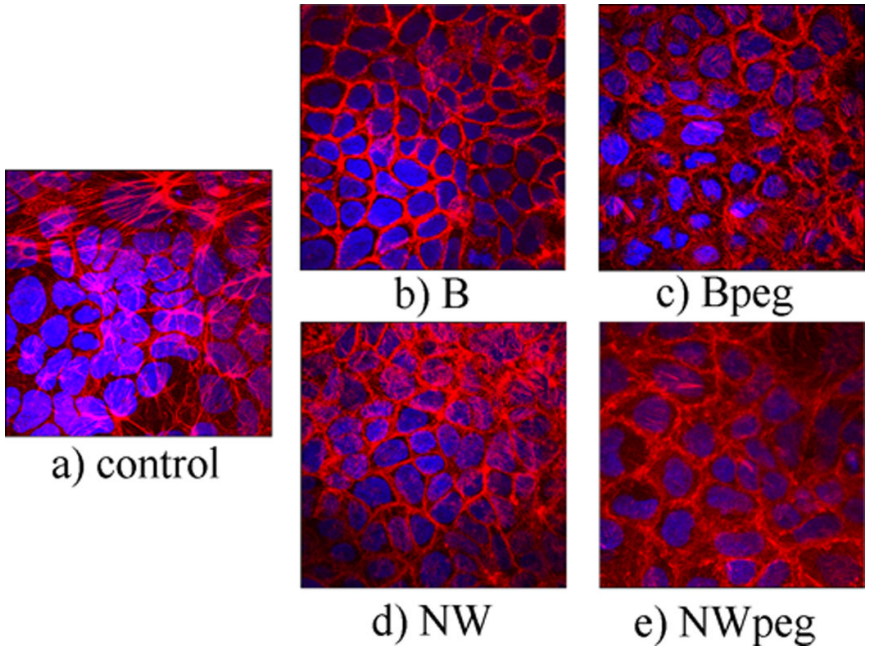

Fig. 4.

Immunoflourescence of untreated Caco-2 cells (a) and those following incubation for 3 h with B (b), B_{PEG} (c), NW (d) and NW_{PEG} (e) counterstained for DAPI (blue), and f-actin (red). All images were taken at 60 × magnification in oil. The size of each image is 450 × 450 μm.

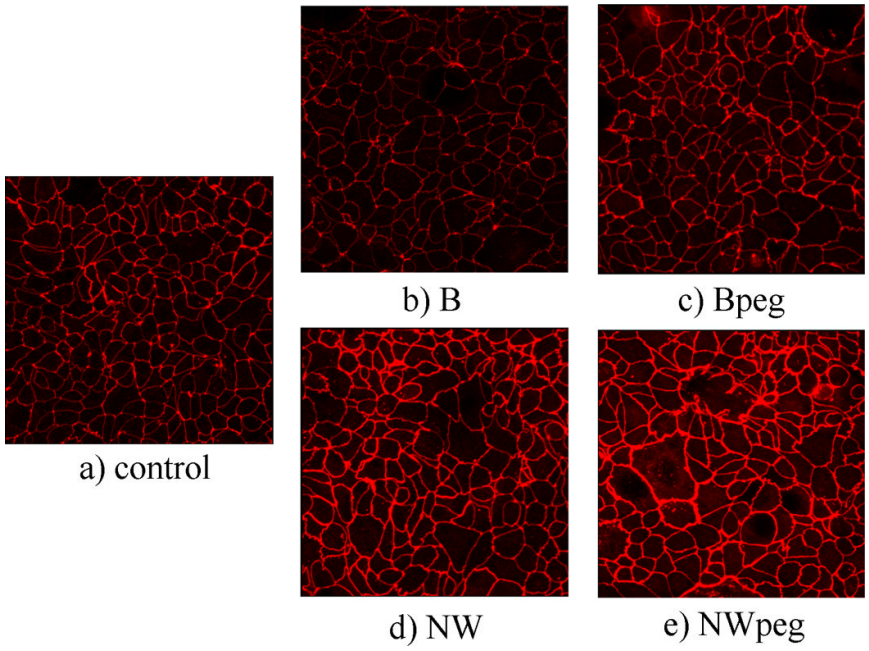

Fig. 5.

Fluorescent staining of ZO-1 molecules in Caco-2 cell monolayers treated for 4 h with: (a) no particles (control); (b) B; (c) B_{PEG}; (d) NW; and (e) NW_{PEG}. The cells were counterstained for ZO-1 (red). All images were taken at 60 × magnification in oil. The size of each image is 450 × 450 μm.

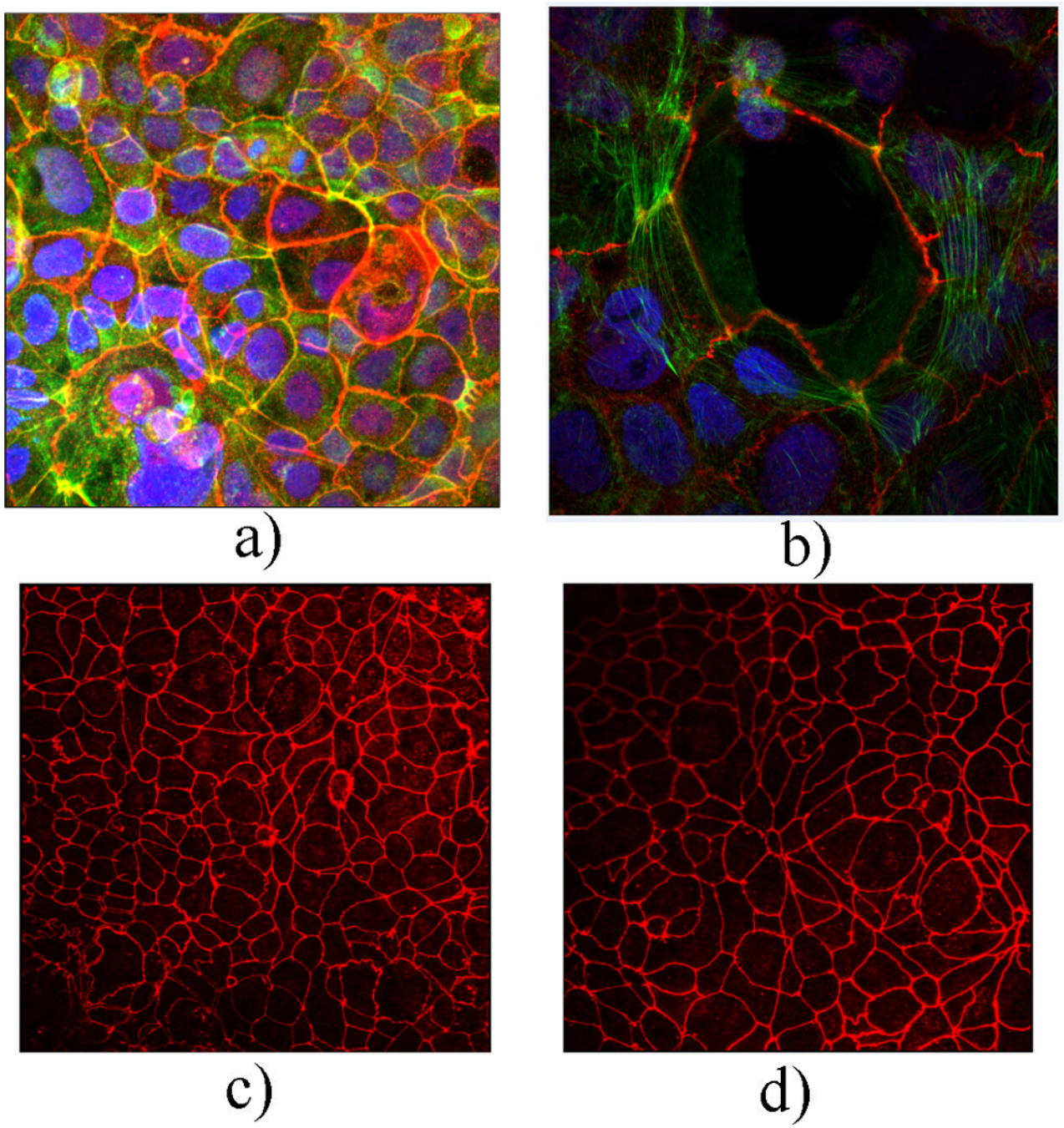

Fig. 6.

Confocal optical micrographs showing: (a) the overlapping f-actin microfilaments (green) and immunostained ZO-1 (red) upon incubation with NW_{PEG}, producing a pattern of yellow color thereby; (b) Caco-2 cell cytoskeleton (green, f-actin), the TJ (red, ZO-1), and cell nucleus (blue, DAPI) in the vicinity of a NW_{PEG} particle (dark area in the center); (c, d) stained ZO-1 pattern in Caco-2 cells incubated with 10 mg (c) and 20 mg (d) of NW particles. The size of the images (a) and (b) is 270 × 270 μm. The size of the images (b) and (c) is 450 × 450 μm.

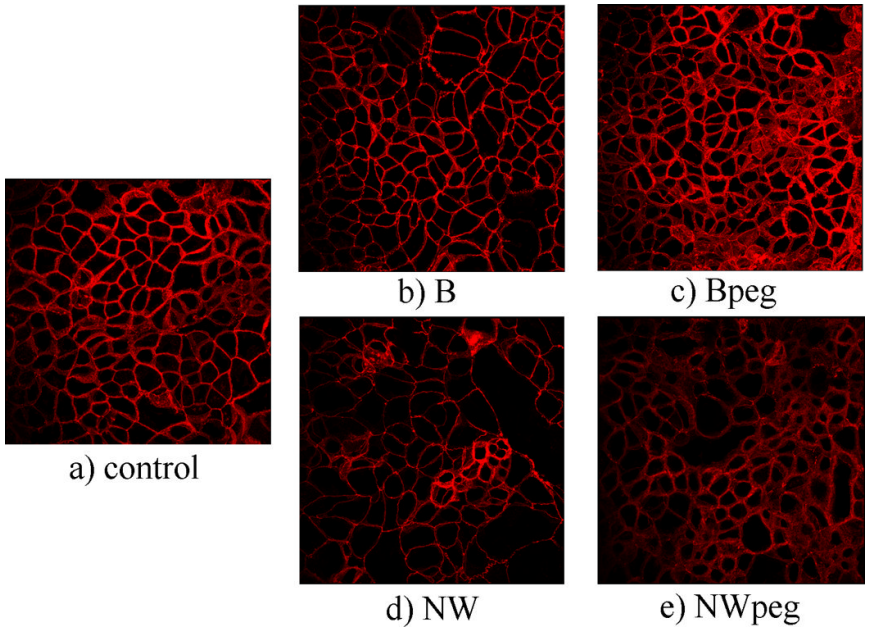

Fig. 7.

Fluorescent staining of claudin-1 molecules in Caco-2 cell monolayers treated for 4 h with: (a) no particles (control); (b) B; (c) B_{PEG}; (d) NW; and (e) NW_{PEG}. The cells were counterstained for claudin-1 (red). All images were taken at 60 × magnification in oil. The size of each image is 450 × 450 μm.

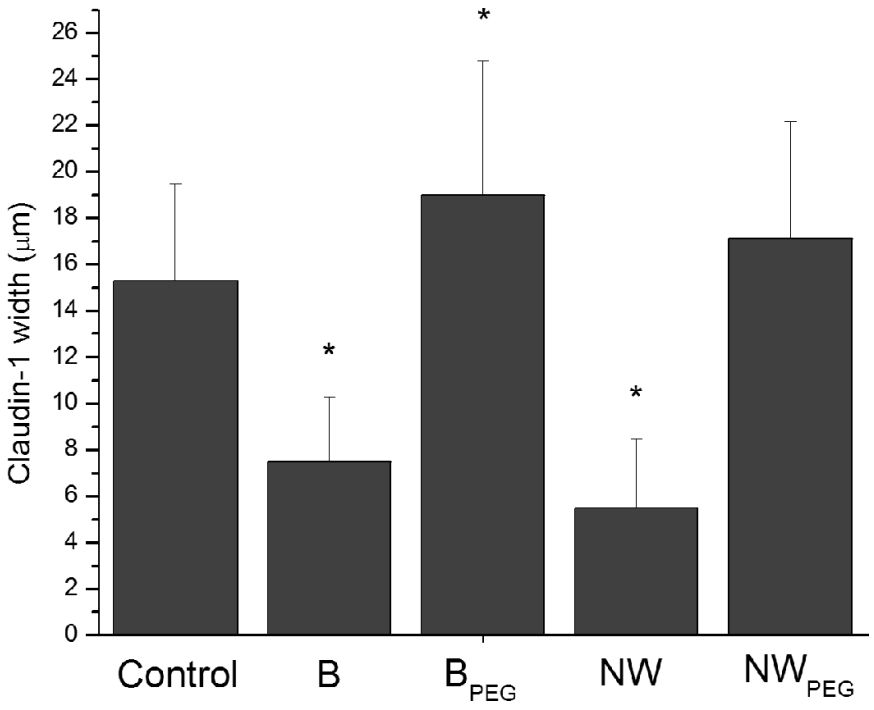

Fig. 8.

Average width of the fluorescent claudin-1 pattern for the control Caco-2 cells and those incubated in the presence of B, B_{PEG}, NW and NW_{PEG}, imaged under identical confocal imaging conditions after 4h of the incubation time. Data are shown as means with error bars representing standard deviation (* => $p < 0.05$ with respect to the control group).

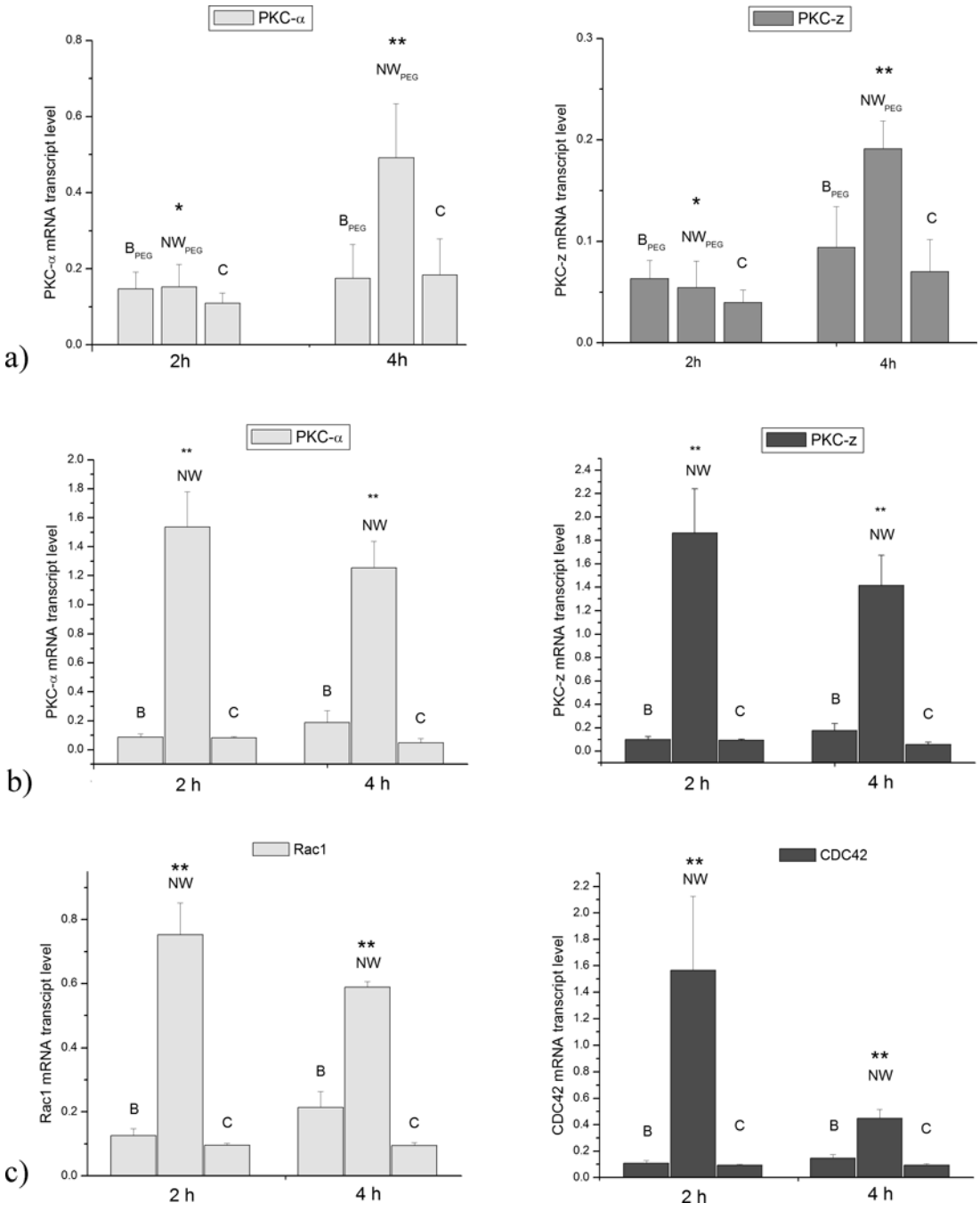

Fig. 9.

The effect of: (a) B_{PEG} and NW_{PEG} particles on the mRNA expression of *PKC*-α and *PKC-z*; (b) B and NW particles on the mRNA expression of *PKC-α* and *PKC-z*; (c) B and NW particles on the mRNA expression of *Rac1* and *CDC42*, all in Caco-2 cells. mRNA expression was detected by quantitative RT-polymerase chain reaction relative to the housekeeping gene *GAPDH*. Data are shown as means with error bars representing standard deviation (* => $p < 0.05$; ** => $p < 0.0001$, with respect to the control group).